1995PASP..107.1234M

Publications of the Astronomical Society of the Pacific
107: 1234–1242, 1995 December

An infrared camera for the Palomar Observatory 60-inch telescope

D. C. MURPHY AND S. E. PERSSON

The Observatories of the Carnegie Institution of Washington, 813 Santa Barbara St., Pasadena, CA 91101
Electronic mail: (david,persson)ociw.edu

MICHAEL A. PAHRE

Palomar Observatory, California Institute of Technology, Pasadena, CA 91125
Electronic mail: map[@000a]stro.caltech.edu

A. SIVARAMAKRISHNAN

The Observatories of the Carnegie Institution of Washington, 813 Santa Barbara St., Pasadena, CA 91101
Electronic mail: anandociw.edu

S. G. DJORGOVSKI[a)]

Palomar Observatory, California Institute of Technology, Pasadena, CA 91125
Electronic mail: george@astro.caltech.edu

Received 1995 June 28; accepted 1995 September 6

ABSTRACT. A near-infrared 0.8–2.5 μm imaging camera for use at the $f/8.75$ Cassegrain focus of the Palomar 60-inch telescope is described. The simple and economical design of this camera is readily adaptable to other telescopes. It features diffraction-limited reimaging optics, high optical throughput (39% at H), and effective K-band background suppression. The camera utilizes an all-reflective, all-spherical optical design that is a variant of the Offner 1:1 reimager. The readout electronics are straightforward, reliable and have low noise, while the data-acquisition system is robust in its utilization of a real-time UNIX operating system on a PC. The electronics and data-acquisition system are described in detail. Various aspects of the performance are given, along with initial results which show that the performance goals of the camera are fully realized.

1. INTRODUCTION

We describe an infrared-(IR) imaging camera built for the Palomar 60-inch $f/8.75$ Ritchey–Chretien telescope. The design requirements for this instrument were driven by three factors. The scientific goals required wide-band imaging data in the 1.2 μm (J-band), 1.6 μm (H-band), and 2.2 μm (K-band) atmospheric windows. The camera was to be built on a relatively modest budget. Finally, we desired a simplified instrument design that could be built quickly (in less than 1.5 years) and that utilized the existing telescope CCD mounting base and offset guider system.

We decided to use a NICMOS-3 256×256 HgCdTe array manufactured by the Rockwell Science Center (Thompson et al. 1989). These arrays are characterized by a high quantum efficiency (as high as QE≈0.7 at K), moderate pixel size (40 μm), low dark current (≈1 e s^{-1}), and high yield. The NICMOS-3 devices are sensitive from 0.8–2.5 μm, which meets our scientific requirements. NICMOS-3 is also simple to clock compared to other IR arrays, and requires cooling to only liquid nitrogen (LN_2) temperature (77 K). The latter feature greatly simplifies the dewar and baffling design. Other factors leading to our selection of NICMOS-3 were its ready availability at modest cost, and our prior successful experience building a system around this detector (Persson et al. 1992).

In Sec. 2 we describe the camera optical design, and in Sec. 3 we describe the mechanical design of the dewar. In Sec. 4 we describe the data-acquisition electronics and computers, including our implementation of the real-time Lynx operating system on the acquisition computers. Finally, in Sec. 5 we summarize the performance of the camera during its first six months of operation, following its commissioning run in 1994 September.

2. CAMERA OPTICAL DESIGN

Reimaging optics in the IR are necessary for a variety of reasons, the most important of which is to provide a stopped exit pupil to prevent thermal radiation originating from regions outside the exit pupil of the telescope from reaching the detector. Sources of this undesirable radiation include the hole in the telescope primary, the secondary spiders, and the annulus around the primary. One solution to this problem is a collimator-camera design based on refractive optics (e.g., Persson et al. 1992). Depending on implementation, such designs have a number of advantages including telecentricity, and the production of a small exit pupil between the collimator-camera elements. Collimator-camera designs are more problematic to implement in the IR than in the optical because multiple-element achromats are required and fewer acceptable glasses exist for IR use than for optical use. Commonly available IR glasses often have poorly determined refractive indices, particularly at cryogenic temperatures.

[1]Presidential Young Investigator.

© 1995. Astronomical Society of the Pacific

© Astronomical Society of the Pacific • Provided by the NASA Astrophysics Data System

1995PASP..107.1234M

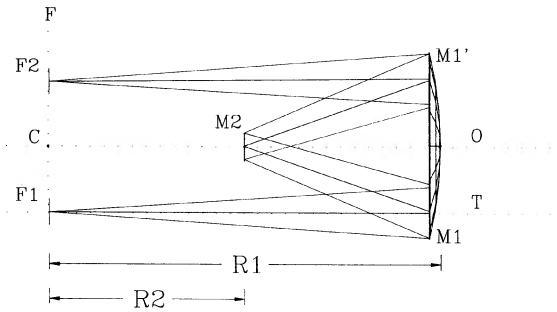


FIG. 1—The Offner reflective optical design. Mirrors M_1 and M_2 are concave and convex, respectively. The focal plane of the telescope is at F_1. Focal planes F_1 and F_2 are coplanar unless the design is folded. The center of curvature is at C. The telescope optical axis is marked by T, while the optical axis of the Offner is marked by O. In our modification of the Offner design, the two illuminated spherical segments of M_1 are separated into concentric mirrors M_1 and M_1' (see also Fig. 2).

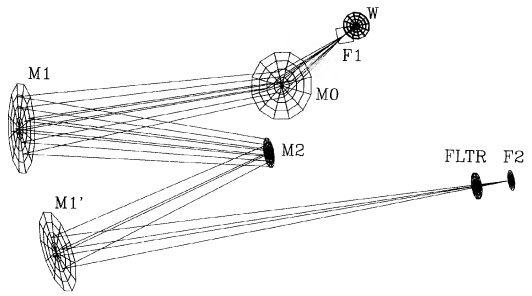


FIG. 2—The final optical design layout corresponding to Table 1. The surfaces are, respectively, a sapphire window (W), a focal plane baffle and stop (F_1), a folding flat (M_0), the convex Offner mirror (M_2), the second concave Offner mirror segment (M_1'), the filter (FLTR), and the focal plane (F_2).

These facts complicate attempts to design cryogenically cooled, near-diffraction-limited reimaging systems for astronomical applications of near-IR arrays.

To avoid such problems we explored various reflective designs for the reimaging optics. Their significant advantage of achromaticity must be weighed against a number of generic disadvantages. For instance, many reflective imaging systems are nonaxial and require one or more aspheric elements, while axial designs suffer from self obstruction. A reflective design that avoids some of these difficulties is the Offner 1:1 telecentric reimager (Offner 1975;Kingslake 1978; Murphy 1994). It is an off-axis, unobscured, all-spherical and all-reflective system. It consists of only two mirrors: a large concave mirror, and a small convex mirror. These manifest advantages are further enhanced by the remarkable characteristic that *the Offner is free from all primary aberrations.* Although the Offner is an off-axis design, and seemingly more difficult to align, in practice alignment has not been a problem.

The concept behind the Offner is illustrated schematically in Fig. 1. In the Offner, the focal and image planes are the same. The design consists of a concave spherical mirror (M_1) and a smaller convex spherical mirror (M_2) with a vertex separation equal to the focal length of M_1. The radius of curvature (of convex) M_2 is half that of M_1 and of opposite sign ($R_2=-R_1/2$). The vertices of the two mirrors are located at a distance equal to their respective radii behind the focal plane (F_1-F_2); in other words, the two mirrors are concentric about a point intersected by the focal plane and a line drawn through the two mirror vertices. Petzval curvature is eliminated since light from the image plane undergoes two reflections at M_1, each contributing Petzval curvature of $P_1 \propto 1/R_1$, and one reflection at M_2, contributing Petzval curvature of $P_2 \propto 1/R_2$. Since $R_2=-R_1/2$, it follows that the total Petzval curvature of a ray traced from the focal plane to the conjugate image plane cancels ($P_{\text{tot}}=2P_1+P_2=0$). The two reflections at M_1 can be thought of as due to two mirrors symmetrical about a stop at M_2. Systems symmetrical about a stop element distortion and suppress coma (Kingslake 1978). Spherical aberration is suppressed because the mirrors are separated by their radii. For illustration, consider the case where both the object and the image point lie on axis. In such a case, ignoring for this example the effect of obstruction, a ray leaving the object point would return exactly to itself simply by geometry. As the object and image points become well-separated and large-angle nonaxial behavior enters, the aberrations (particularly astigmatism) increase. Nevertheless, the Offner clearly represents an attractive starting point for developing a wide-field IR reimager.

The nature of the exit pupil formed by the Offner presents certain subtleties that must be considered. An image of the telescope primary, and essentially all telescope structure which is approximately at "infinity," is formed *by* mirror M_1 *at* mirror M_2 (since $f_1=D_{12}=R_1/2$) (Fig. 1). Thus essentially M_2 *is the pupil stop for the system.* It is desirable that this image be as free from aberrations as possible so that effective pupil masking can be achieved. An undersized stop will suppress an ill-defined "fuzzy-edged" pupil and lose light, while an oversized stop will admit unwanted background radiation. The image of the telescope primary mirror formed at M_2, essentially that of an extended object located at "infinity," suffers spherical and other aberrations. Also, because the axis of the Offner is offset half the diameter of M_2 (i.e., $d_1/2$) from the axis of the telescope, and the virtual image of the primary formed behind the telescope secondary is a finite distance from M_1, the image of the primary formed at M_2 is not precisely centered on the M_1–M_2 axis. In our particular implementation the pupil image is slightly nonconcentric by a linear amount of order $\approx$1.2 mm with respect to the M_2 vertex.

The above considerations led to a modified design, in which mirror M_1 has been separated into two spherical mirrors M_1 and M_1' (Figs. 1 and 2). These two mirrors represent the illuminated spherical segments of a larger mirror. This separation was desirable in our implementation for several reasons. First, the size of the concave mirror in the Offner is determined by the scale of the entire system and the degree to which the focal/image plane is off-axis, i.e., the separation of focal and image points made to avoid central obstruction. A larger separation, whoever, produces a more aberrant image, and the larger this separation, the larger the M_1 diameter becomes (Fig. 1). Therefore, ideally, the diameter of M_1 should be just large enough to accommodate the image plane size without vignetting by M_2. However, in initial tracing studies, it was found that it was possible for stray radiation at

© Astronomical Society of the Pacific • Provided by the NASA Astrophysics Data System

1995PASP..107.1234M

TABLE 1

Detailed optical design.

Surface	Radius [a] (mm)	Displacement [b] (mm)	Thickness [c] (mm)	Glass.	Index[d]	Dia. [e] (mm)
Tel. Primary [f]	−7619.977		2827.918	mirror		1524.0
Tel. Secondary [g]	2750.003		3407.316	mirror		454.6
Dewar Win. W	–		2.000	Sapphire	1.74446	25.40
Air Space			28.565			
Focal Plane F_1 and Stop			157.209			
Flat M_0 [h]	–		195.000	mirror		56.70
Mirror M_1 [i]	−350.000		174.601	mirror		71.40
Mirror M_2	171.86	45.000	168.810	mirror		23.90
Mirror M_1' [i]	−344.491	90.000	312.414	mirror		65.80
Filter FLTR (K_s)	–	90.000	1.118	Silicon	3.47022	25.40
Air space			25.000			
Focal plane F_2	–	91.680				

[a]Negative radius indicates concave surface.
[b]Displacement of the surface vertex off-axis.
[c]Denotes distance to subsequent surface.
[d]Index of refraction at H (1.65 μm).
[e]Full aperture.
[f]Asphere with conic constant −1 and sag=$(-6.5617\ 10^{-5})\ y^2+(1.835\ 10^{-14})\ y^4$ mm.
[g]Asphere with conic constant −1 and sag=$(-1.818\ 10^{-4})\ y^2+(1.743\ 10^{-11})\ y^4$ mm.
[h]Folds beam 90°.
[i]Surfaces M_1 and M_1' are tilted 7.387° about their vertices towards S_5 (toed-in).

large angles (>3.3°) originating from sources at infinity to strike M_1, pass above M_2, and fall directly on the array. Several measures were taken to avoid this possibility in the actual system: (1) The separation of focal and image planes (92 mm) was made to be an amount larger than that required simply to prevent vignetting by the convex mirror; (2) A stringent 5% oversized focal plane stop was employed to help suppress off-axis thermal radiation, with a 114 mm long baffle tube following the focal plane stop; (3) An annular stop around M_2 (in addition to a precisely machined stop for the secondary support arms and hole in the telescope primary) was used; and (4) a baffle tube extending from the array to the plane of M_2 was employed.

Apart from stray radiation suppression, separation of concave mirror M_1 into smaller segments has further advantages. More degrees of freedom are allowed in the design because the radii, tilts, and vertex positions of these mirrors are now parameters. In particular, separating M_1 into two mirrors allows one to better optimize the pupil plane image (see below). It also reduces the vertical height of the optics, thus reducing the dewar volume. Finally, two small precision mirrors are cheaper than one larger one.

To deal with the problem of a decentered pupil mentioned above, tracing results showed that the pupil image could be recentered on M_2 by introducing a tilt of the entire camera about the focal plane of ≈0.35°. A tilt of this magnitude abberates the focal plane image to a negligible extent. Screw adjustments allowing a tilt of up to 1.5° were incorporated into the base plate which mounts the dewar to the telescope allowing pupil alignment to be performed at the telescope. Best alignment of the pupil image onto M_2 corresponds to minimal K-band background.

Optimization toward a final design was performed after the above points were borne out by preliminary tracings. All ray tracing was performed using the commercial program ZEMAX (Focusoft, Tucson, AZ). Optimization was done with designs fed by an accurate model of the telescope. This allowed an accurate evaluation of the final image, as well as balancing of inherent telescope aberrations by the camera optics. The design process was begun by taking the classical Offner and splitting the concave mirror M_1 into two spherical segments with appropriate tilts and vertex locations. The first spherical segment, M_1, was then shifted parallel to the optical axis by the optimization algorithm (holding other variables constant), to provide the smallest spots possible *in the pupil plane* tangent to the vertex of M_2. The "objects" for pupil plane optimization were points taken at the inner and outer annuli of the primary mirror. Of course, the pupil-plane optimization degraded the focal plane image. To compensate for this, the *optimization of the focal plane image* was then performed by varying the position of M_1' along the optical axis, the back focus, and the radii of M_2 and M_1', but holding the parameters affecting the pupil-plane image constant (e.g., the M_1 to M_2 vertex separation). The design was then checked for its effectiveness at suppressing stray radiation. The vertex separation of M_1 and M_1' (perpendicular to the optical axis) was then manually varied to trade off focal/pupil plane image quality versus stray radiation baffling effectiveness and the design process was iterated until no stray light could be forced onto the array. Each design was exhaustively checked for vignetting as well, and considerable attention was paid to the optimal sizing of the apertures at each iteration.

The final design is presented in Fig. 2 and Table 1. The scaling for the optical layout was driven by the following practical consideration: the Palomar 60-inch is an f/8.75 Richey–Chretien with a focus ≈35 mm below an instrument mounting base (IMB) originally designed for CCD cameras. This area is crowded with an offset guider and other apparatus forcing us to mount the dewar 76 mm below the IMB.

© Astronomical Society of the Pacific • Provided by the NASA Astrophysics Data System

1995PASP..107.1234M

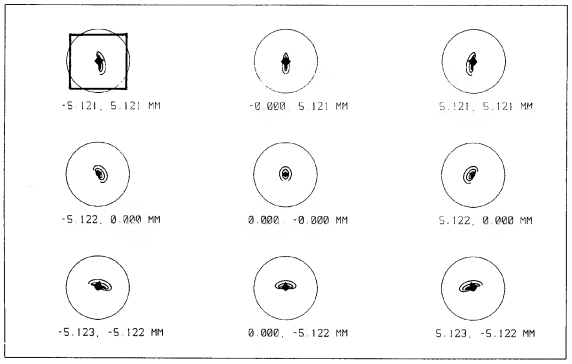


FIG. 3—Spot diagrams made at λ=-2.2 μm (K_s) for objects at the center, edges, and corners of the field. The spot positions are labeled by their (x,y) positions on the array in mm. The circles represent the diameter of the first dark ring of the Airy diffraction disk. Also shown for the spot at the corner of the array at (−5.121 mm, 5.121 mm), is a 40 μm×40 μm square representing a NICMOS-3 pixel. Note the highly corrected nature of the design.

This in turn required a relatively long total length of 1034 mm for the optical path of the reimager (measured from F1 to F2, Figs. 1 and 2). The specification we have given in Table 1, while rather complete, excludes many details of baffles (for economy of presentation). Note that the optics are folded 90° by flat FLT in order to fit within the dewar (discussed below). The final design reflects many tradeoffs. The ray tracing includes the effect of all filters which we tilted at 5° to the incident light to throw-off multiple reflections. Despite the fact that our filters are in a converging beam, tracing results, confirmed by experience at the telescope, show that for filters of interest, variations in spot size induced by optical thickness differences (between filters) were not significant with respect to image spread due to seeing.

The predicted performance of the optical system is illustrated in Fig. 3 where calculated spots at λ=2.2 μm for field points at the center, edges, and corners of the array are shown. For reference, a circle representing the diameter of the first dark ring of the Airy diffraction pattern (at λ=2.2 μm) is drawn superposed on the spots. The Strehl ratio, a measure of how close a system is to being diffraction limited, is 0.95 for the central field point; a Strehl ratio greater than 0.8 indicates a diffraction limited design (Smith 1990). The excellent optical performance out to the corners of the array immediately suggests an Offner-style design for cameras with larger arrays. We have indeed verified a diffraction limited design very similar to the present one, aimed at the next generation HgCdTe array from Rockwell, a 1024×1024 device with 18.5 μm pixels.

The mirrors, manufactured by Janos Technology (Townshend, Vermont), were specified to be accurate to 1/4λ peak-to-valley (P–V) at 0.63 μm. The figured clear aperture of the mirrors is 95% of the full aperture. The figured clear aperture in turn exceeds the aperture which would vignette by ≈7%. These selected apertures, while conservatively oversized, ensured that vignetting could not occur and that rays encountered only accurately figured surfaces. The mirrors are made of Zerodur because of its insensitivity to thermal contraction effects and its workability, although the material choice is not critical. The mirrors were coated with protected silver (a Janos process) to achieve an estimated reflectivity of at least 97% per mirror throughout the 0.8–2.5 μm wavelength range of the camera.

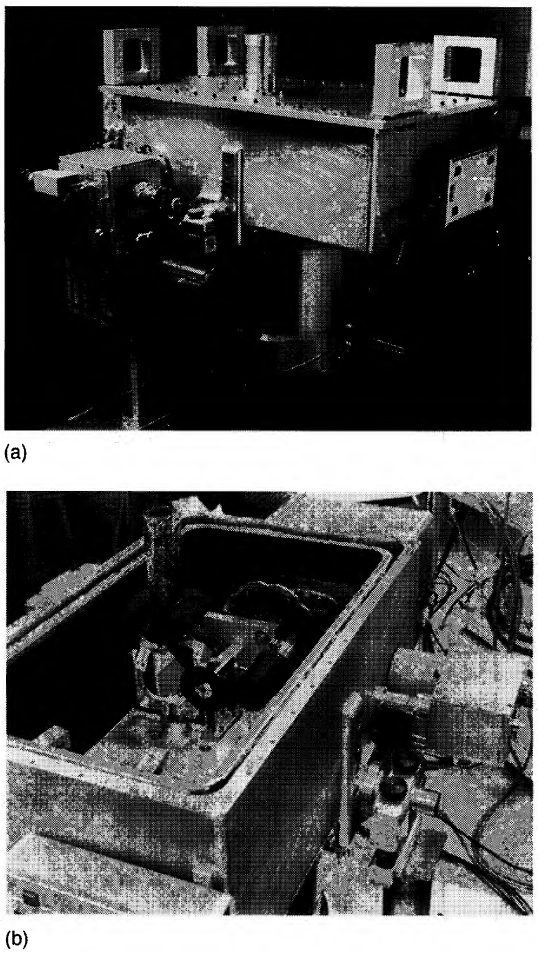


FIG. 4—Two views of the camera dewar. View (a) is an exterior view of the dewar resting on its handling cart which allows a 180° rotation about pivots. In this orientation the entrance window is pointed up. In View (b) the dewar cover has been removed to show the optical bench. Mirror M_2 and its stops are clearly visible. Flat M_0 and a baffle extending above it is also seen. Just barely visible to the lower left are the tops of mirrors M_1 and M_1' and their mounts. To the right of M_2 is a baffle extending from its plane to the filter wheel. Behind the filter wheel is seen a portion of the dewar wiring card. The filter wheel motor is seen exterior to the dewar at the right hand side of the photograph.

3. DEWAR MECHANICAL DESIGN

Figure 4 shows photographs of both the interior and exterior of the dewar. The optics are mounted on a rectangular optical bench. The vertex of M_2 defines the optical axis—it is not adjustable in any fashion. M_1 and M_1' are kinematically mounted with spring-loaded plungers squeezing the mirror against screws with 80 threads per inch. A laser was used to set the angular alignment of the optical surfaces, while the linear vertex separations were constrained by the precision of the machining. Also mounted on the optical bench are the filter wheel gearing/detent mechanism, light

© Astronomical Society of the Pacific • Provided by the NASA Astrophysics Data System

1995PASP..107.1234M

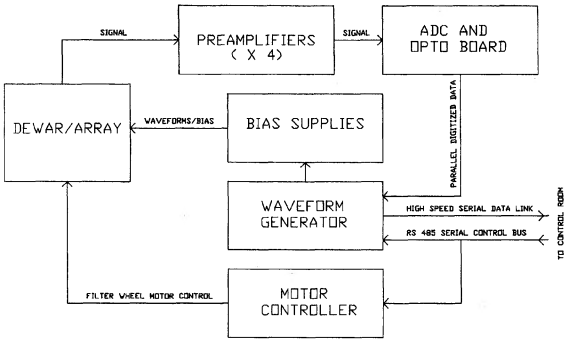


FIG. 5—Block diagram of the camera electronics.

baffles, detector wiring card, and the adjustable mount for flat M_0 [Fig. 4(b)]. Eight filter positions are available, although one of these is blocked off to form a dark shutter.

The portion of the dewar enclosing the optical bench is an aluminum box that extends the outer can of an IR Labs (Tucson, AZ) LD-10 dewar. Likewise, the radiation shield is extended up to a rectangular aluminum box, and the inner work surface up to the optical bench. The LD-10 dewar is configured to work upside down so that at the telescope it hangs underneath the rectangular box. Three electrical plugs enter the evacuated dewar—one for the clocks, one for the dc bias voltages, and one for the signals. The time required to completely disassemble the optical bench and detector mount is about 1/2 hour.

Selection of a black paint for the inside surfaces of the dewar was made in consultation with K. Matthews (Cal Tech), who made extensive tests of various combinations of primer and overcoat. A primer from Cardinal Industrial Finishes (South El Monte, CA) was found to work well with a black overcoat that is unfortunately no longer available. We therefore elected to use the primer with Cardinal's Velvethane Solar Optical Black overcoat, which appeared on a test sample to be reasonably black visually. This was deemed to be a reasonable approach because the reduction of scattered thermal radiation within the dewar is not a severe problem for short wavelength cutoff HgCdTe arrays.

4. ELECTRONICS AND DATA ACQUISITION

4.1 Overview

A block diagram of the electronics is given in Fig. 5. There are six subsystem enclosures: the dewar/array, the preamplifiers, the analog-to-digital converter (ADC) and optoisolator boards, the bias supplies, the waveform generator (WFG), and the motor controller. The main function of the electronics is to read-out the array (a four quadrant device) by digitally clocking it while amplifying and digitizing its signals. To avoid excessive expense and complication, our system biases and clocks all four quadrants simultaneously, although ti si possible to digitize data from only one quadrant if desired (e.g., for fast readout modes). The array electronics are physically located in enclosures bolted to the dewar. Control of the electronics occurs via RS-485, an industry standard multidrop serial data bus similar in some respects to RS-232. Digitized data from the dewar electronics are sent to the acquisition computer remotely located in a control room via a simple custom-built high-speed serial data link (3 megabits s^{-1}). The functional details of NICMOS-3, relevant to understanding the full motivation for the electronics, are discussed briefly by Thompson et al. (1989) and are available from Rockwell.

The detailed functioning of the electronics is summarized as follows. An integration sequence begins when the acquisition computer sends an ASCII command to the WFG over the RS-485 line (Fig. 5). The WFG, a microprocessor-based unit, begins to clock all four array quadrants simultaneously. The four outputs of the NICMOS-3 on-board amplifiers are then simultaneously preamplified and digitized by the 16 bit ADC. After digitization, the data are sent in a custom serial format to a frame buffer on the acquisition computer. After necessary preprocessing, such as forming double-correlated pictures, the acquisition computer logs the image to the Sun disk.

4.2 Dewar/Array Wiring

The array itself is mounted in a 68-pin ceramic chip carrier designed to mate with a commercially available plastic leaded chip carrier socket (PLCC socket). A spring-loaded clamp/optical baffle holds the array chip carrier tightly onto the PLCC socket, which is itself mounted on a Rockwell provided circuit board. All dc voltages were filtered with capacitors added to this board (wired in a point-to-point method) following Rockwell specifications. Metal film resistors were also added to complete internal array analog circuits such as source followers. All dc, clock, and signal voltages are brought on or off the array circuit card to hermetic connectors via stainless-steel coaxial cable (Lake Shore Cryotronics, Westerville, OH). The board is clamped thermally—but not electrically—to the cold optics mounting plate. LakeShore heat sinks were used for this purpose.

4.3 Analog Signal Processing and Biasing

The preamplifiers are designed to remove a $\approx$4 V offset from array voltage and amplify it a factor of 21.5 in preparation for digitization. The input stage of the preamplifiers uses the Burr Brown (Tucson, AZ) INA103BG low-noise instrumentation amplifier for initial gain. This is followed by a dc offset removal stage based on the OP27EP op-amp. The subtracted dc voltage is derived from a National Semiconductor (Santa Clara, CA) LM199 voltage reference, a device distinguished for its stability (Horowitz and Hill 1989). The last stage constitutes an 8-pole 100 KHz cutoff Bessel filter based on OP27EP's designed following Horowitz and Hill (1989). This filter provides noise suppression, bandwidth narrowing, and anti-aliasing. A Bessel filter was chosen because of its relatively distortion-free time response, important to prevent pixel blending.

The amplifiers are built on individual custom designed four-layer PC boards following low-noise layout methodology. Precision metal film resistors and polystyrene or polycarbonate capacitors with low-temperature coefficients were used throughout. Each board has separate on-board voltage

© Astronomical Society of the Pacific • Provided by the NASA Astrophysics Data System

1995PASP..107.1234M

regulation, an approach designed to minimize the possibility of cross-talk between quadrants. The preamplifier boards are built into a custom enclosure mated directly to the dewar via a multipin military-style hermetic connector. In practice the preamplifier has proved stable, reliable, and easy to adjust.

The preamp outputs are sent to the ADC board, which contains four sample-and-hold (SH) amplifiers and one ADC. Careful attention to low-noise electronic engineering is necessary to ensure a reliable ADC subsystem that does not exchange noise with other components of the electronics. Our ADC board, designed by Bruce Atwood at Ohio State University (and also used in their IR instrument OSIRIS) utilizes the Burr-Brown 16 bit ADC/SH 701/702 chip set. It incorporates power-supply isolation, on-board voltage re-regulation, and ferrite-bead basednoise suppression filters on power input lines. The ADC board is built on a 3U X 220 mm Eurocard. To isolate the ADC, and generally to keep digitally produced WFG ground noise from entering the ADC board or other parts of the signal chain, we opto-isolated all digital lines entering or leaving this board. The Opto-isolators reside on a separate board adjacent to the ADC board in the same enclosure. To increase the isolation between the ADC board and the rest of our electronics, the ADC power supplies were separated and not shared with the rest of the electronics. All power supplies for the ADC (and our electronics in general) are high quality, stable, low-noise linear supplies.

The bias enclosure houses the analog and digital bias boards—which supply array power and waveform voltages. The analog bias board is dedicated to providing stable, low-noise dc analog bias voltages. These bias voltages are referenced to a National LM369BN voltage reference, whose output is level shifted and filtered with a low frequency cut-off ($f_c \approx 1$ Hz) low-pass op-amp based active filter. The filtered reference voltage is, in turn, distributed to individually adjustable low-pass buffer-filter output channels. Outputs to the array have voltage-limiting diodes and transient suppressors to protect the array. The OP27EP operational amplifier was employed for all active functions on both bias boards. The analog bias board provides the ability to digitally switch off the bias voltage (SOURCE) supplying the on-array source follower output amplifier during longer integrations. This may reduce on-array amplifier glow, but we have not found this useful in practice. We currently operate the array with all nonzero bias voltages at 5 V except for the detector reverse bias voltage (DETBIAS) which is set at 0.90 V. We have verified that both well-depth and dark current correlate with DETBIAS.

The function of the digital bias board is to take WFG clocks, opto-isolate and level shift them, and then supply them to the array. The opto-isolation prevents fluctuating ground current from the noisy, current-consuming, WFG board from finding a ground path through array grounds. The digital bias board also supplies the array with dc voltages used to power digital array functions. The boards are housed in a custom enclosure mated directly to the dewar with a military-style connector carrying only dc voltages to the array. The clocks enter the dewar through a physically separate military-style connector after a short cable jump from the enclosure. This circuitous routing isolates the noisier clock signals from the more sensitive dc voltages.

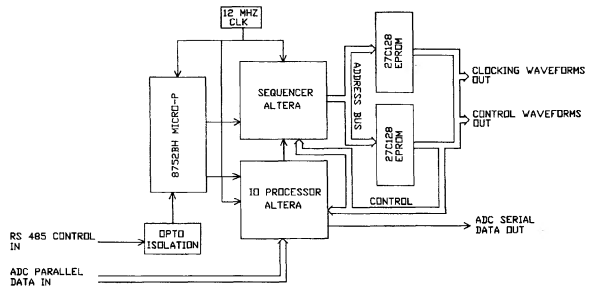


FIG. 6—Block diagram of the waveform generator (WFG) circuit.

4.4 The Waveform Generator Board (WFG)

The WFG board produces clocks for the array and synchronously-driven system circuitry like the ADC. After weighing various considerations, including cost, the occasional need to change and experiment with different waveform patterns, and firmware development system issues, we decided to adopt an EPROM-based circuit.

Figure 6 gives a block diagram of the WFG circuit. While based on the conservative approach of utilizing EPROM's to generate clocking patterns, we implemented several features to enhance our ability to reconfigure this circuit. First, the circuit is supervised by an Intel 8752BH micro controller (Intel, Santa Clara, CA). Second, two high density erasable–programmable logic devices (EPLD's; Altera Corp., San Jose, CA) are used to implement most logic functions, replacing ≈45 TTL chips that would otherwise have been required. Third, a graphical wave-form editor was developed to display and edit EPROM waveforms on an IBM-compatible PC prior to burning. This program, written in C, and operating interactively in graphics mode, eased the task of generating and modifying waveforms. This editor presents a time-ordered display of the clocking waveforms similar to that of a logic analyzer. The folding of many logic functions into 8752 firmware or directly into the EPLD's allowed us to build the WFG on a single 115×150 mm board.

The WFG operates as follows. The acquisition computer sends the WFG instructions over the RS-485 line coded as a two character ASCII command with optional argument. A typical command would set the integration time or initiate a double correlated integration. The 8752 assumes full control over integrations. For instance, on double correlated sequences the 8752 will first trigger an array clocking with reset-off, followed by another clocking with reset-on, followed by the integration time, and then followed by a final clocking. The 8752 does not directly generate waveforms, but triggers counter circuits that address EPROM waveform memory. The 8752 code, developed in C (about 800 lines), does not run under an operating system, guaranteeing that integration timing loops are always exactly the same number of 12 MHz clock pulses long. The 8752 disables *all* interrupts during double-correlated integration sequences so that strictly accurate, repeatable hardware timing is always ensured. This hardware timing approach is easy to implement,

© Astronomical Society of the Pacific • Provided by the NASA Astrophysics Data System

1995PASP..107.1234M

and is significantly more reliable than the commonly used technique of frame timing under control of a computer running an operating system. The latter method forces one to deal with the complex issue of latency times. Our approach eliminates this worry entirely and assures precision timing. This is particularly important if good photometry for short exposure times is to be obtained.

The waveforms employed are stored in EPROM's in a bank-switched fashion. There are four banks, or sets of patterns, available. Waveform generation occurs when the 8752 sets a bit that gates-in pulses (divided form the 12 MHz clock) to decoded counters in the Sequencer Altera that drives EPROM address lines. The 8752 maintains programmable control over the speed of EPROM clocking. Frame times as short as a few milliseconds to as long as many seconds are possible, although the bandwidth of the rest of our system limits the shortest double correlated integration time to 405 ms for one quadrant, or 743 ms for all quadrants. A final WFG function performed by the IO Processor Altera is to latch parallel ADC bytes and send them in a serial stream to the remotely located acquisition computer. This simple (custom) serial data link runs at 3 megabits s^{-1} utilizing 50 ohm coaxial cable.

4.t Motor Control

The single filter wheel is controlled by a simple motor/gearbox/detent design. The mechanical detents ensure exact repeatability of filter positions, a requirement for accurate sky subtraction. The spring-loaded detents are located on the wheel itself inside the dewar. The filter wheel is driven by an encoded externally mounted two-phase ac motor that is geared down in two steps.

The motor controller is built around an Intel 8752BH micro controller, programmed in C. Commands to the motor controller can be sent either via RS-485 or by an increment/decrement manual override switch mounted on the controller housing. The motor controller reads positional information from the encoders on the gear shaft and opens ac relays to drive the motor as necessary. In addition to the manual override switch, the filter wheel may be positioned by hand in the event of a complete failure of external electronic/computer control.

4.6 Computer Architecture

Factors motivating the data system design were: (1) that the system have sufficient processing power and memory to handle the image sizes and expected data rates; (2) that the system adhere to proven hardware/software standards; (3) that it be economical; and (4) that the software be straightforward to develop and use.

To facilitate these goals, we decided on a two-computer physical architecture employing standard PC and Sun Sparc computers running UNIX operating systems and X/Motif windowing environments. All acquisition software was developed in the widely accepted C language. A key advantage of UNIX is that it allows device driver development to be readily performed in C. We chose to perform all image processing on the Sun using IRAF. Adherence to these standards avoids unnecessary duplication of effort and takes advantage of the powerful tools of UNIX/X/Motif/IRAF.

The control and acquisition computer, an 80486 66-MHz PC, has a 520 megabyte SCSI disk and 16 megabytes of RAM. The analysis computer is a Sun Sparc 2 with 64 megabytes of memory. The Sparc 2 is used by the observer to interact with a camera control window and the usual Sun IRAF software interface. The two computers communicate over an Ethernet LAN (RG 58A/U Thinlan).

By using two computer systems we best utilize the capabilities inherent in each machine. For example, the Sparc 2 and Sun OS, while excellent for running IRAF, are ill-suited for hardware interfacing and fast real-time data acquisition. In contrast, the PC and its buses (e.g., ISA-Industry Standard Architecture) are well-supported in terms of interface cards, drivers, etc., and are well-documented open systems in terms of interface knowledge. On the PC we run Lynx-OS (Lynx Real-Time Systems, Los Gatos, CA), a UNIX compatible operating system. This system has enhancements to improve the real-time response of application program.s Such response is useful since our frame timing is performed by the WFG, thus the acquisition computer must synchronize itself with externally driven timing events that vary greatly with the length and type of integration performed. We note that Lynx OS has also been found useful by other groups for applications in astronomy (Rayner et al. 1993; Spillar et al. 1993).

The logical architecture of our system is that of " one" computer. The acquisition program executing on the PC, projects its window across the network via X/Motif to display on the Sparc. The observer is not even aware of the PC (which resides physically below the observing floor in the facility's computer room) since he/she interacts solely with windows on the Sun. To ease observing set-up, Sun login scripts automatically start all necessary windows, including the remote starting of the camera acquisition program which then transmits its window across the network.

4.7 Data Acquisition

Three components comprise the acquisition program: (1) an X/Motif user interface, (2) code to acquire, process, and store images, and (3) code to control the filter-wheel motors. Another major, but logically separate software component, is a UNIX kernel-level device driver for servicing the frame buffer.

The camera window holds a palette of variables defining (primarily) integration parameters. After setting these parameters, the user begins an integration sequence by mouse clicking the START button. The PC then downloads the parameters via RS-485 to the WFG and commands an integration. At the interface level, frames of converted data flow from the WFG-produced high-speed serial data stream to the PC's frame buffer card (developed at OCIW), mounted in a slot of the PC. The frame buffer takes the data stream, unserializes it back to parallel 16-bit ADC conversions, and stores the 16-bit words in a 64 K-word-on-board RAM buffer. After an entire NICMOS-3 frame is stored, the frame buffer issues an interrupt signalling that the buffer is full and

© Astronomical Society of the Pacific • Provided by the NASA Astrophysics Data System

1995PASP..107.1234M

needs servicing. The acquisition program (via the device driver) then empties the buffer using programmed I/O bus cycles, which we found to be considerably faster (≈4 Megabytes s^{-1}) than traditional ISA direct memory access (DMA). Our frame buffer approach, while simpler than the more modern technique of a FIFO for fast data streams, *guarantees* in a software independent fashion that no data are lost due to the momentary inability of the computer to keep pace with the data stream.

Data frames, having been acquired by the acquisition program from the interface card, are held and processed in RAM on the PC (they *never* touch the PC's disk). After preprocessing, which might, for example, consist of double correlated subtraction or end-point averaging, an IRAF compatible disk file of the image is written to a directory located physically on the Sparc disk, but co-mounted by the PC using Network File Services (NFS). The same co-mounted directory is pointed to by IRAF running on the Sparc, allowing the observer to examine acquired data immediately. This powerful technique is similar to that exploited by Nadeau et al. (1994). This method furthers the integration of the two physically distinct computers into one logical computer. For instance, from the programmer's viewpoint, the seemingly complex operation of shipping large amounts of data error-free from one machine to the other is performed simply by ordinary high-level file handling calls.

4.8 System Tests

We have found it possible to perform noise tests on NICMOS-3 with the array *at room temperature* by reading the array with the RESET line asserted, i.e., by taking reset pictures. A pair of reset pictures may be subtracted to form a frame suitable for studying read noise statistics. Read noise measurements taken using this technique are essentially the same as when the array is cold. This method has proven to be extremely convenient since one may experiment at will with the grounding and power distribution internal to the dewar circuitry without the need to effect a dewar cycle. This technique is also a useful system check before cooling the dewar.

5. CAMERA PERFORMANCE

The camera was put into operation in 1994 September. The overall performance of the camera is summarized in Table 2, where measurements of CIT–CTIO IR standard stars were used for calibration (Elias et al. 1982).

There are no obvious problems with the camera optics at the telescope, although it is only possible to perform consistency checks on the (excellent) theoretical expectations discussed above because of the moderately coarse 0.62 $pixel^{-1}$ scale. Fits to stellar profiles are consistent with theoretical expectations for this pixel scale at all points on the array.

One of the most important engineering tasks during the first session was the minimization of the thermal background reaching the array from improper alignment of the entrance pupil onto mirror M_2 (Fig. 2). This misalignment may arise from effects in addition to those inherent in the optical design discussed in Sec. 2 above such as warping of the camera body at cryogenic temperatures, and telescope collimation errors. Alignment was achieved by measuring the sky background level in the K_s filter and iteratively adjusting the camera tilting screws. Only a few iterations were needed to find the minimum.

TABLE 2
Camera Performance Summary

	J	H	K_s	Units
Wavelength	1.25	1.65	2.15	μm
Bandwidth (FWHM)	0.25	0.30	0.33	μm
Throughput [a]	0.26	0.39	0.34	e^- $photon^{-1}$
Background [b]	15.82	14.09	13.57	mag $(arcsecond)^{-2}$
Limiting Magnitudes [c]	21.10	20.20	19.50	mag

[a]In units of e^- out of the array per photon in at the top of the atmosphere. This includes transmission losses of the atmosphere, telescope, camera optics, filters, and detector QE.
[b]Sky backgrounds are representative for J and H, where variations, particularly at H, can amount to a factor of two during a typical night. The K_s background is very respectable; it was measured at an ambient/telescope temperature of 0 °C.
[c]For a 2.5 arcsecond diameter aperture, signal-to-noise of 5:1, and integration time 3600 s. This represents a typical "deep" measurement.

The barely sufficient image sampling afforded by the pixel scale raises the question of how precise the photometry of the stars can be. This depends mostly on the effective fill factor: if no light falling on the pixel boundaries were lost, the issue might be less important. We have reduced the data from several observing runs, and we find there is a negligible loss of precision compared to our data taken with our camera at Las Campanas which operates at scales of 0.35 or 0.42 arcseconds $pixel^{-1}$ (Persson et al. 1992). typical one-sigman dispersions of the magnitudes of bright stars measured at four positions on the array (of the camera described here) are 0.005 mag.

The pixel scale of the camera was measured using the precise positions of 75 stars in the globular cluster M15 (provided by K Cudworth). A least-squares solution under the assumption of no distortion gives a scale of 0.6200 ± 0.0004 arcseconds $pixel^{-1}$ for J, H, and K_s. This is in good agreement with the value predicted from ray tracing of 0.618 arcseconds $pixel^{-1}$. Based on measurements of stars in M13, the rms distortion over the entire field is ≈0.1 arcseconds.

Electronically, the camera performs close to expectations. We realize a read noise of 40 e^- rms for one double correlated read, with no end-point averaging. Experimentation with averaging a number of reads at the beginning and end of an exposure shows that for up to $N=9$ reads the read noise reduction varies roughly as $\sqrt{N}$. We have observed no cross talk between quadrants in any readout mode. The well depth at a reverse bias voltage of 0.9 V is of order 2.5×10^5 e^-. When integrating, we typically keep our signal levels below 1.8×10^5 e^-. In conditions of good seeing this poses a problem in that CIT–CTIO IR standard stars are too bright to observe in integrations exceeding 1 s. To deal with this problem we have implemented a fast readout mode of one quadrant with a 405 ms integration time. The latter mode is useful for stars a little brighter than 7th magnitude (J, H or K).

The particular NICMOS array made available for this project is quite good cosmetically. There are several low QE regions which flat field well. The nonlinearity of the array

© Astronomical Society of the Pacific • Provided by the NASA Astrophysics Data System

1995PASP..107.1234M

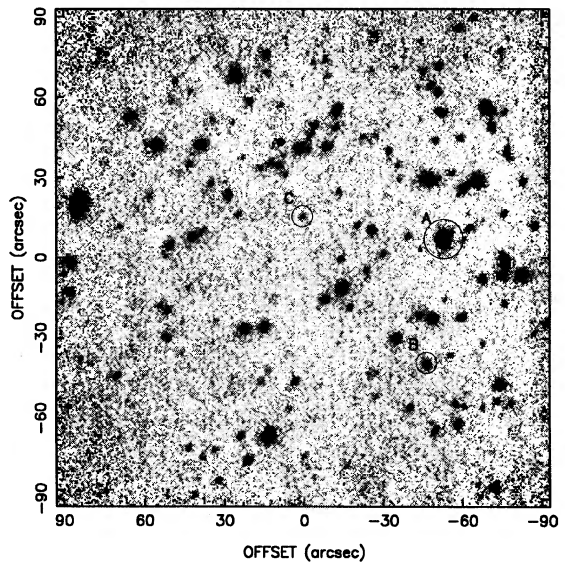


FIG. 7—K_s image of the core of $z=0.41$ cluster Abell 851. This image, taken during February of 1995, represents a stack of reduced images with a total integration time of 5100 s. The data were acquired in groups of 5×60 s integrations on each of 17 positions spaced 15 arcseconds apart. In this image north is up and east is to the left. The center position is $(\alpha, \delta)=(9^h43^m2.6^s, 46°58'57'')_{2000}$. Three faint galaxies in the image are identified to demonstrate the camera performance. Their measured magnitudes in a 5″ diameter aperture are: $K_s=15.26\pm0.01$ (A), 16.89 ± 0.03(B), and 18.55 ± 0.12 (C), where the uncertainties indicate photometric errors.

response was measured and found to be typical for NICMOS-3, viz., about 4% over a range of signal from zero to two-thirds of saturation. This small effect is easily dealt with in reduction, though a future upgrade of the data acquisition software will linearize the frames on line.

Persistence, or residual after-images of bright stars, seems to be a generic problem with NICMOS-3 arrays. To suppress persistence we read the array with the RESET line asserted (i.e., we reset the entire array) every two seconds except when performing an integration. This function is performed automatically by the WFG.

During the first six months of operation, the camera has been used for a variety of scientific programs including: the establishment of a set of new $K=11$ IR standards; K-band imaging of elliptical galaxies in nearby rich clusters; selection of a $K=20$ field galaxy sample for a spectroscopic redshift survey; main-sequence fitting in JHK for galactic clusters with Cepheid variable stars; imaging of rich clusters at $z=0.1$ to 0.4; JHK imaging of local-group galaxies to investigate both their stellar populations and surface-brightness fluctuations; IR photometry of high-redshift radio galaxies and quasars. We present a representative image from this instrument for the core of the $z=0.41$ cluster Abell 851 in Fig. 7.

We would like to thank Kadri Vural, Duc Bui, Scott Cabelli, and Bob Bailey of Rockwell for their extensive help and advice regarding detector issues. We acknowledge generous support from the Perkin Fund, the Jeanne Rich Foundation, Rockwell International Corporation, NSF Grant No. AST-9123646, and NSF/PYI award No. AST-9157412. M.A.P. acknowledges partial support from Greenstein and Kingsley Fellowships. We acknowledge the support and participation of Jeremy Mould in the early stages of the development of this instrument. We acknowledge the considerable contribution of our machinists L. Vasquez, B. Storts, J. Dizon, and P. Ramirez. We thank D. Carr for designing the motor controller electronics. The frame buffer card was designed by I. Thompson and S. West. We thank B. Atwood at OSU for designing and building the ADC board. We acknowledge influential discussions concerning computer interfacing issues with S. Shectman. We thank F. Perez for advice on mechanical and vacuum issues. We thank H. Petrie of Palomar Observatory for providing information on the optical and mechanical design of the 60-inch telescope. We thank M. Sekiguchi for providing useful source code to assist in writing IRAF compatible image files. We thank the Palomar Mountain crew for providing essential support during all our observing runs. We acknowledge the work of E. Koch in designing the preamplifier PCB's. We thank S. Majewski for his help in assembling the preamplifiers. We thank J. Cohen for providing an analysis of the camera distortion. D.C. M. acknowledges the influence of electronic and data-acquisition design ideas from previous generations of IR cameras constructed at the university of Arizona, NOAO, and the University of Montreal.

REFERENCES

Elias, J. H., Frogel, J. A., Matthews, K., and Neugebauer, G. 1982, AJ, 87, 1029

Horowitz, P., and Hill, W. 1989, The Art of Electronics, 2nd ed. (Cambridge University Press, Cambridge)

Kingslake, R. 1978, Lens Design Fundamentals (Orlando, Academic)

Murphy, D. C. 1994, in Infrared Astronomy with Arrays: The Next Generation, ed. I. McLean (Dordrecht, Kluwer), p. 301

Nadeau, D., Murphy, D. C. Doyon, R. and Rowlands, N. 1994, PASP, 106, 909

Offner, A. 1975, Opt. Engineering, 14, 130

Persson, S. E., West, S. C., Carr, D. M., Sivaramakrishnan, A., and Murphy, D. C. 1992, PASP, 104, 204

Rayner, J., et al. 1993, Proceedings of the SPIE, Infrared Detectors and Instrumentation, ed. Albert M. Fowler (Bellingham, WA, SPIE), Vol. 1946, p. 490

Smith, W. J. 1990, Modern Optical Engineering, 2nd ed. (New York, McGraw-Hill)

Spillar, E. J., Dumbrill, D., Grasdalen, G. L., and Howell, R. R. 1993, PASP, 105, 616

Thompson, R., Rieke, M., Young, E., McCarthy, D., Rasche, R., Blessinger, M., Vural, K., and Kleinhans, W. 1989, Proceedings of the Third Infrared Detector Technology Workshop, ed. C. R. McCreight (NASA Technical Memorandum 102209), p. 331

© Astronomical Society of the Pacific • Provided by the NASA Astrophysics Data System